

# Magnetostriction in the $J$ - $K$ - $\Gamma$ model: Application of the numerical linked cluster expansion

Alexander Schwenke \* and Wolfram Brenig †

*Institute for Theoretical Physics, Technical University Braunschweig, D-38106 Braunschweig, Germany*

(Dated: November 21, 2025)

We apply the numerical linked cluster expansion (NLCE) to study thermodynamic properties of the proximate Kitaev magnet  $\alpha$ -RuCl<sub>3</sub> on the honeycomb lattice in the presence of a magnetic field. Using the extended spin-1/2  $J$ - $K$ - $\Gamma$  model and based on documented exchange and magnetoelastic coupling parameters, we present results for the internal energy, the specific heat, and the magnetization. Moreover, the linear magnetostriction coefficient perpendicular to the plane is calculated, which is sensitive to changes of the in-plane spin-spin correlations. We find the magnetostriction to display a dip-like feature, in line with the temperature dependent and field-driven suppression of magnetic order in  $\alpha$ -RuCl<sub>3</sub>. Our results are consistent with previous findings, establishing NLCE also as a tool to study magnetoelastic features of quantum magnets.

## I. INTRODUCTION

Mixing spin- with lattice-degrees of freedom is relevant to a wide range of features of magnets [1], including, e.g., thermodynamic and critical properties [2], cooperative phenomena [3], as well as phonon and ultrasound renormalization [4]. In this context, magnetostriction, i.e., the relative change of lengths  $L$ , with applied magnetic fields,  $\Delta L/L(H)$  is a quantity of great interest in magnets with frustration, since in these the magnetic properties can depend sensitively on the geometry [5–11].

Recently, frustrated quantum magnets with Ising interactions that are bond-dependent by virtue of the exchange quantum-chemistry have become of great interest. On the honeycomb lattice and for spin-1/2 they give rise to the celebrated Kitaev model [12]. This model harbors one of the few known quantum spin liquids (QSL) in two dimensions (2D). This QSL displays fractionalization of spins into mobile Majorana matter and  $\mathbb{Z}_2$  gauge flux excitations (visons) [12–15]. The visons are localized in the absence of external magnetic fields. The ground state is flux-free and displays gapless fermionic quasiparticles with a Dirac spectrum. All spin correlations are short ranged [16].

Mott-Hubbard insulators with strong spin-orbit coupling [17], like  $\alpha$ -RuCl<sub>3</sub> [18], have been suggested as candidate materials, proximate to the Kitaev model. However, non-Kitaev exchange interactions lead to zigzag antiferromagnetic order below 7.1 K in this material [19]. Applying an in-plane magnetic field  $H$  along the Ru-Ru bond direction,  $H\parallel b$ , first induces a transition between different interplane zigzag orderings at  $H\parallel b = H_{c1} \sim 6.4$  T, before suppressing order completely [20, 21], producing a quantum disordered range of  $H\parallel b = H_{c2} \sim 7.1 \dots 11$  T  $\sim H_{c3}$  which might host the sought for low-temperature QSL [22–26]. Excitation continua observed in several probes, both, direct, i.e., Raman [27–

29], inelastic neutron [30–33], and resonant X-ray scattering [34], as well as indirect, i.e., phonon spectra [35–41], and ultrasound attenuation [42, 43], have been attributed to fractionalization in  $\alpha$ -RuCl<sub>3</sub>.

In view of the potential QSL which emerges from the zigzag order by increasing temperature and magnetic field, identifying the proper low-energy Hamiltonian for  $\alpha$ -RuCl<sub>3</sub> is very important. To this end, various spin models have been suggested [44–58], which include additional off-diagonal and Heisenberg exchange,  $\Gamma_i$  and  $J_i$ , respectively, beyond the pure Kitaev coupling  $K$ . Each of these exchange parameters can be sensitive to stress or strain and thereby impact magnetoelastic probes. In  $\alpha$ -RuCl<sub>3</sub> this relates, e.g., to spin-phonon scattering matrix elements [35–43] and to the mixing between magnetic and phononic thermal transport modes, both, longitudinal and transverse [23, 59–61]. Moreover, and as one prime motivation for the present study, this is relevant to interpreting the field-induced transitions in  $\alpha$ -RuCl<sub>3</sub> probed by the structural Grüneisen parameter and magnetostriction [62–64].

The observed magnetostriction displays pronounced and temperature dependent anomalies in the vicinity of  $H_{c1,c2}$  [62, 64]. As of today, this has been described theoretically by linear spin-wave theory [62] and by exact diagonalization [63]. In this situation, and as a second motivation of this work, we aim at considering the magnetostriction of  $\alpha$ -RuCl<sub>3</sub> as a testbed for a third, and complementary computational method, namely, the NLCE [65, 66].

The NLCE is based on the linked cluster theorem and allows calculating quantities in the thermodynamic limit without the need for finite size scaling. In contrast to other series expansions [67] and also earlier LCE approaches [68], the NLCE is non-perturbative, relying on exact diagonalization (ED) to obtain the contributions from each individual cluster to the thermodynamic limit. This method has been applied previously to analyze a wide range of spin and general quantum many body systems for their ground-state [69, 70], thermodynamic [65, 66, 71–75], and dynamic [76, 77] properties. Beyond that, it has been used to study entanglement entropies

\* a.schwenke@tu-braunschweig.de

† w.brenig@tu-braunschweig.de

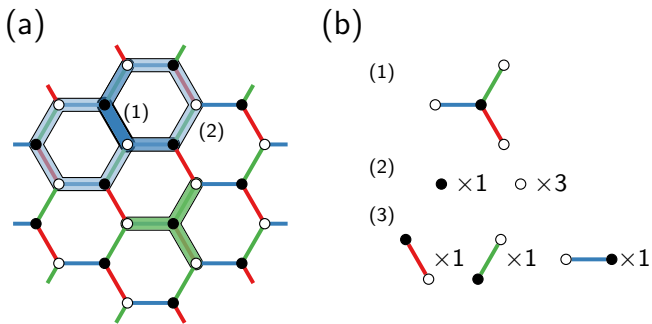


FIG. 1. (a) Honeycomb lattice and sample clusters thereon. Red, green and blue label x-, y- and z-type bond-directional exchange, respectively. Black and white vertices denote the triangular lattice basis. Smaller clusters such as (1) can be fully contained by larger ones such as (2). (b) NLCE-decomposition of a cluster into its constituent exemplified: Tricoordinated unit (1) consists of four sites (2) and, equivalently of three bonds (3), one of each type.

at quantum critical points [78, 79], quantum phase transitions [72, 80–83], fermions in optical lattices [84–87], inhomogeneous [88] and disordered systems [89], as well as others [90–93]. We note, that apart from the NLCE, another successful cluster approach to spin models exists, namely the coupled-cluster-method (CCM) [94–96]. While the CCM is an exponential-Ansatz bivariational approach, which is rather different in spirit from the NLCE, both methods share the remarkable common feature of being constructed directly to satisfy the linked-cluster theorem.

In this work we will use the NLCE to obtain thermodynamic properties, and in particular the magnetostriction of  $\alpha$ - $\text{RuCl}_3$ . The paper is organized as follows: In Sec. II we describe the  $J$ - $K$ - $\Gamma$  model. Sec. III summarizes the NLCE method and our implementation. In Sec. IV we provide our results, including the energy, specific heat, and magnetization in Secs. IV A, IV B, and IV C, respectively, before discussing the magnetostriction, in IV D. We summarize in Sec. V.

## II. MODEL

We consider the spin  $S=1/2$   $J$ - $K$ - $\Gamma$  model, which is an extension of Kitaev’s original Hamiltonian, adapted to a more realistic description of spin-orbit coupled magnets

$$H = \sum_{\substack{\langle ij \rangle \parallel \gamma, \\ \alpha \neq \beta \neq \gamma}} [J \vec{S}_i \cdot \vec{S}_j + K S_i^\alpha S_j^\beta + \Gamma (S_i^\alpha S_j^\beta + S_i^\beta S_j^\alpha)] + \vec{h} \cdot \vec{S}, \quad (1)$$

where  $\vec{S}_i$  are spin-1/2 operators residing on the sites  $i$  of the honeycomb lattice,  $\vec{S} = \sum_i \vec{S}_i$  is the total spin, and  $K$  and  $J$  refer to the Kitaev and Heisenberg exchanges respectively,  $\Gamma$  is an off-diagonal exchange and  $\vec{h}$  is an external magnetic field.  $\vec{h}$  relates to the experimentally

n Topo.		n Topo.		n Topo.	
1	1	6	55	11	7008
2	3	7	125	12	19756
3	3	8	360	13	55097
4	10	9	919	14	156357
5	18	10	2588		

TABLE I. Number of topologically distinct clusters up to the 14th expansion order on the honeycomb lattice with bond directional nearest neighbor interactions

accessible field  $\vec{B}$  via  $\vec{h} = \mu_B g \vec{B}$  with the Bohr magneton  $\mu_B$  and the  $g$ -tensor. The sum on  $\langle ij \rangle$  extends over nearest neighbor bonds of the honeycomb lattice. The bond-directional nature of the interactions is indicated in Fig. 1(a), where x-, y-, and z-type bonds are colored red, green, and blue, respectively. On a given bond along the  $\gamma$ -direction, the Kitaev interaction couples the  $\gamma$ -components of the spins, while the  $\Gamma$  interaction couples the remaining two components  $\alpha \neq \beta \neq \gamma$ .

The  $J$ - $K$ - $\Gamma$  model has first been suggested as a minimal model for the iridium oxide family  $A_2\text{IrO}_3$  ( $A = \text{Na}, \text{Li}$ ) and can be obtained via a strong coupling expansion of a multiorbital  $t_{2g}$  Hubbard-Kanamori Hamiltonian [97]. Shortly thereafter, the same model has been proposed for  $\alpha$ - $\text{RuCl}_3$  [18]. Various sets of exchange parameters have been put forward in the literature [44–58, 63]. Here we use the set of Ref. [63] which has been obtained by extensive ab-initio analysis. We note that in the latter Ref. further exchange interactions have also been considered. However, for the present work, and the sake of simplicity, we restrict ourselves to  $J$ ,  $K$  and  $\Gamma$ . In turn, we use the following set of model parameters  $\{J, K, \Gamma\} = \{-0.564, -1.0, 0.92\} \times |K|$  with an overall energy scale of  $|K| = 10.1$  meV.

## III. NLCE: APPLICATION TO THE HONEYCOMB LATTICE

Our method of choice, i.e., the NLCE [65] is based on the linked cluster theorem (LCT) [67], which states that for any observable  $\mathcal{O}$  representing an extensive quantity, the thermodynamic average can be written as

$$\langle \mathcal{O} \rangle / N = \sum_{c \in \mathcal{L}} L(c) W_{\mathcal{O}}(c), \quad (2)$$

where the summation extends over all connected clusters  $c$  that can be embedded in the lattice  $\mathcal{L}$ ,  $N$  is the number of lattice sites,  $\langle \dots \rangle$  refers to the trace over the density matrix, and  $L(c)$  and  $W_{\mathcal{O}}(c)$  are the multiplicity and the weight of a cluster  $c$ , respectively.

$L(c)$  is a purely geometrical quantity. It depends only on the shape of the cluster and is given by the number of times  $c$  can be embedded in  $\mathcal{L}$ , without taking into account translations, i.e., per site. In contrast to that,  $W_{\mathcal{O}}(c)$  depends on the observable  $\mathcal{O}$  and can be

understood as the irreducible contribution of the cluster  $c$  to  $\langle \mathcal{O} \rangle$ . It is obtained recursively using the inclusion-exclusion-principle:

$$W_{\mathcal{O}}(c) = \mathcal{O}(c) - \sum_{s \subset c} W_{\mathcal{O}}(s). \quad (3)$$

This recursion guarantees that  $W_{\mathcal{O}}(c)$  comprises only correlations such that all sites of the cluster  $c$  are connected. Rearranging the LCT by cluster size, (2) reads

$$\langle \mathcal{O} \rangle / N = \sum_{n \in \mathbf{N}} \sum_{c \in C_n} L(c) W_{\mathcal{O}}(c), \quad (4)$$

where  $C_n$  contains all linked clusters of size  $n$  embeddable in  $\mathcal{L}$  which are not related by translations. Disconnected clusters do not contribute to 4 because of 3. Also note that the cluster size  $n$  is not necessarily identical to the number of sites but can rather be defined with respect to arbitrary building blocks, e.g., bonds or plaquettes.

The NLCE then consists of truncating 4, hence approximating

$$\langle \mathcal{O} \rangle / N = \sum_{n < n_{\max}} \sum_{c \in C_n} L(c) W_{\mathcal{O}}(c) \quad (5)$$

with  $n_{\max}$  sufficiently large and using ED to evaluate  $W_{\mathcal{O}}(c)$  numerically.

Since clusters that host the same Hamiltonian and therefore the same density matrix do not need to be considered individually, finding and eliminating topologically identical clusters is crucial for lowering the computational cost of the NLCE. In order to do so, we use the graph automorphism library `nauty` [98].

Typically, the number of topologically distinct clusters,  $n$ , as well as the Hilbert space dimension of the clusters grow exponentially with the order of the expansion. Indeed, from Table I, for the honeycomb lattice  $n \propto e^{\alpha n}$  with  $\alpha \approx 1.04$ , for  $n \gtrsim 4$ . Depending on the lattice  $\mathcal{L}$  and available computational resources, this sets a limit on the maximum order,  $n_{\max}$ , accessible by NLCE. Yet, beyond this truncation order, and as with all approximations that are of series expansion type, the convergence of the bare NLCE sum of Eq. (5) can be improved in many cases by making use of resummation techniques [91, 99]. In this work we employ the Euler transformation and compare results for  $n = n_{\max}$  and  $n = n_{\max} - 1$  to ensure convergence.

The Euler transform considers a sequence of finite sums  $S_k = \sum_{n=0}^k a_n$  and maps them to a new one, i.e.,  $\tilde{S}_j = s_{j,0}$ , where  $s_{j,k}$  is defined recursively by

$$s_{0,k} = S_k, \quad s_{j+1,k} = \frac{s_{j,k} + s_{j,k+1}}{2}. \quad (6)$$

$\tilde{S}_j$  either converges to the same value as the original series  $S_j$  as  $j \rightarrow \infty$  or does not converge at all.

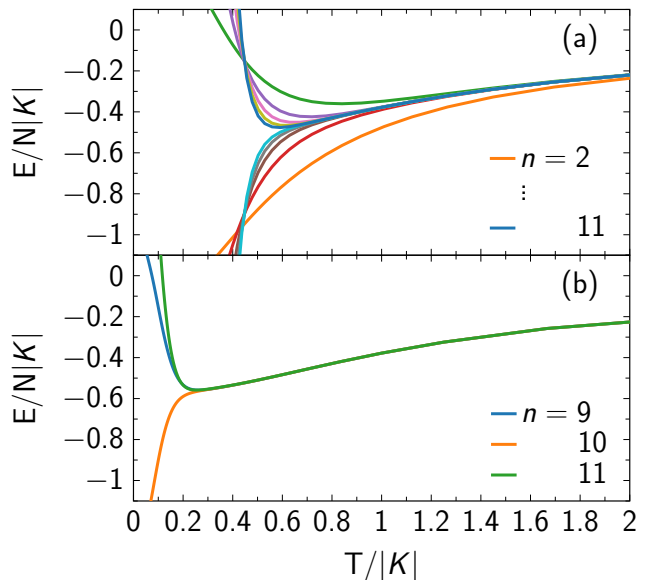


FIG. 2. (a) Internal energy per site in the  $J$ - $K$ - $\Gamma$  model calculated using bare sums and (b) the Euler resummation

## IV. RESULTS

In this Section we present our results for the  $J$ - $K$ - $\Gamma$  model. This includes the internal energy, specific heat, magnetization, and finally the magnetostriction coefficient. One emphasis of the discussion is on analyzing the NLCE versus different expansion orders and respective Euler transforms, in order to study the convergence properties. Additionally we contrast the NLCE against results from ED, obtained on finite clusters with periodic boundary conditions. We note that in the following we refer to the magnetic field as  $B$  to avoid confusion with the Hamiltonian  $H$ . However, the critical field values in  $\alpha$ - $\text{RuCl}_3$  are usually referred to as  $H_{c1,2,3}$ , therefore we will use the same notation when discussing these.

### A. Internal energy at $h = 0$

The internal energy  $E = \langle H \rangle$  comprises the thermal average of the local spin correlations accumulated by the Hamiltonian Eq. (1). The transition into the zigzag phase in  $\alpha$ - $\text{RuCl}_3$  is second order. Therefore, one expects the internal energy to be a continuous function of  $T$  even if the NLCE would converge down to  $T = 0$ .

Fig. 2 shows  $E$  per site versus temperature. As is obvious from panel (a), up to the orders considered, the bare NLCE is converged down to  $T \approx 0.6|K|$ . In order to improve this convergence of the NLCE, we apply the Euler transform in panel (b). While the bare expansions diverge in an alternating fashion below  $T \approx 0.6|K|$ , the Euler transforms of the NLCE at orders  $n = 10$  and  $n = 11$  agree down to  $T \approx 0.25|K|$ . Speaking differently, we may conclude that the series of Euler transformed ex-

pansions has converged down to this temperature range. While this is a considerable increase of the range of validity, the lowest temperature of  $0.25|K|$  is still clearly above the Néel temperature  $T_N \simeq 7$  K of  $\alpha$ -RuCl<sub>3</sub>. Therefore the results Fig. 2(b) are well within the paramagnetic phase.

### B. Specific heat at $h = 0$

We obtain the specific heat from the mean square of the energy fluctuations

$$C_V = \frac{\partial E}{\partial T} = \frac{\langle H^2 \rangle - \langle H \rangle^2}{k_B T^2}. \quad (7)$$

The numerator on the right-hand side is an extensive quantity and therefore accessible to NLCE.

We evaluate  $C_V$  up to order  $n_{max} = 11$  at  $h = 0$ . In Fig. 3(e) Euler resummations for  $n = 10, 11$  are shown together with results from full spectrum ED on 12 (Fig. 3(a),(b)) and 16 site (Fig. 3(c),(d)) clusters using periodic boundary conditions. This figure allows to clearly observe both, strengths and weaknesses of the NLCE. Regarding the former and as determined by the convergence of the resummation, NLCE is able to reach the thermodynamic limit down to  $T \gtrsim 40$  K on clusters of only 11 sites. This is very different for the ED. As is obvious, ED does not only display significant finite size effects, but also substantial variations versus cluster shape at fixed cluster size. Only cluster (d) is close to the thermodynamic limit within all of the range of convergence of the NLCE, requiring however a Hilbert space larger by a factor of 32.  $C_V$  on this cluster properly reproduces the position of the hump at  $T \sim 75$  K and is only slightly too small for  $40 \text{ K} \lesssim T \lesssim 70 \text{ K}$ . Clusters (b) and (c) shift the hump to a higher temperature of  $T \sim 85$  K and overestimate  $C_V$  up to  $T \sim 160$  K, while cluster (a) displays an overall shape and location of characteristic features significantly off from the NLCE and all other ED results. Cluster shapes (a) and (b) have been used in a study of the specific heat of the Kitaev-Heisenberg model, i.e., at  $\Gamma = 0$  [100]. However for the parameters employed here, Fig. 3 demonstrates that clusters (c) and (d) are more suitable. For all remaining comparison to NLCE, we use only the larger of those clusters, i.e., (d).

As for NLCE's weakness, the low-temperature divergent behavior of the resummation below 30 K is obvious. Here, around  $T \sim 10 \text{ K} \sim 0.1|K|$  and on clusters (c)-(d) ED displays a second 'hump' of various intensity. Rephrasing all of this, NLCE typically allows reaching a controlled thermodynamic limit on clusters smaller than those required for ED. Below the low-temperature convergence however, NLCE is not defined, while ED results may still be interpreted, accepting possibly considerable finite-size effects.

The existence of two humps in  $C_V$  at  $T \sim 75 \text{ K} \sim 0.65|K|$  (NLCE and ED) and at  $T \sim 10 \text{ K} \sim 0.1|K|$  (ED)

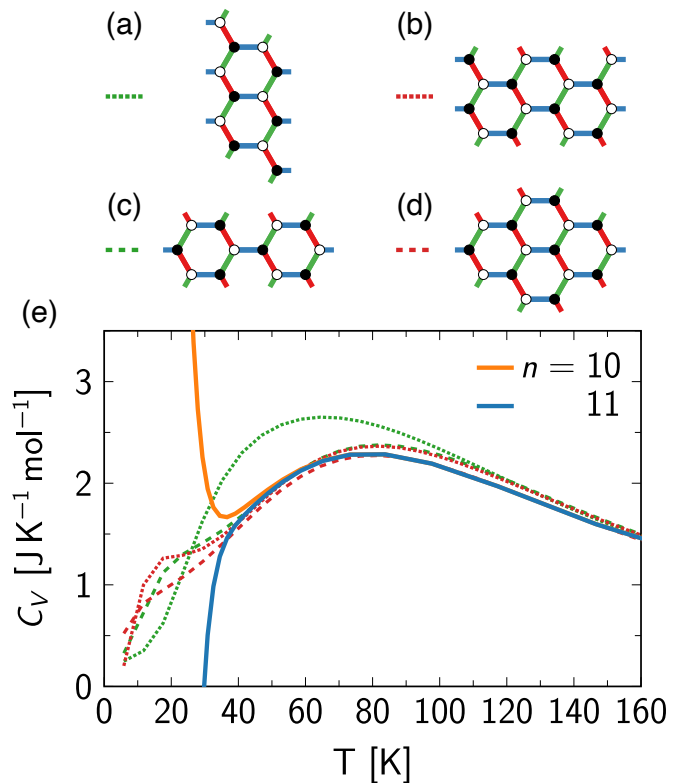


FIG. 3. (e) Specific heat of the  $J$ - $K$ - $\Gamma$  model: Comparison of 10th and 11th order NLCE (solid orange and blue), with ED on clusters of 12-sites (green dotted/dashed, (a)/(c)) and 16-sites (red dotted/dashed, (b)/(d)).

in Fig. 3 could be related to the physics of fractionalization in the pure Kitaev model [12] at  $J = \Gamma = 0$ . In that case the specific heat displays two maxima [101, 102], i.e., a high-temperature peak, which is located at  $\sim 0.6|K|$  and is associated with the entropy of Majorana fermions and a low-temperature peak owing to the proliferation of gauge visons at  $\sim 0.05|K|$ . We caution however, that no obvious relation exists between fractionalization in the pure Kitaev model and the double peak structure in  $C_V$ . In fact, the so-called  $\Gamma$  model for  $\Gamma \neq 0$  but  $J = K = 0$  displays similar features in  $C_V$  [103] which persist for a broad range of  $\Gamma, K \neq 0$  [104]. Yet, the Kitaev spin liquid state is known to be severely unstable with respect to  $\Gamma$  exchange interactions [97].

### C. Magnetization

Experiments on  $\alpha$ -RuCl<sub>3</sub> have shown a significant anisotropy of the magnetic susceptibility with respect to the orientation of the applied magnetic field [105, 106]. For a Kitaev-Heisenberg model, i.e., a  $K$ - $J$  model, this difference can be explained allowing for a substantial  $g$ -tensor anisotropy [54] which originates from strong trigonal distortion [107]. Including however an off-diagonal  $\Gamma$  interaction allows for an alternative mechanism. In

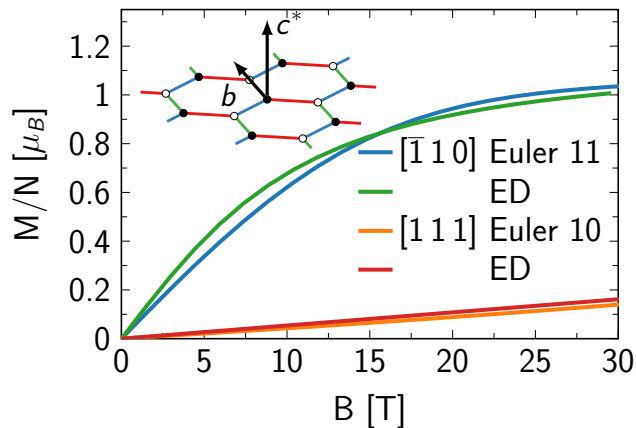


FIG. 4. Comparing NLCE versus ED for the magnetization of the  $J$ - $K$ - $\Gamma$  model at  $T = 29.3$  K for magnetic fields with in-plane, i.e.,  $[\bar{1} 1 0] \hat{=} b$  and out-of-plane, i.e.,  $[1 1 1] \hat{=} c^*$  directions. ED on cluster Fig. 3(d).

fact,  $\Gamma$  acts as an antiferromagnetic coupling along the out-of-plane  $c^*$ -direction but as a ferromagnetic coupling for spins that are aligned in-plane [49] - see the inset in Fig. 4 regarding the conventions for field directions. This difference automatically leads to a smaller magnetic response in the  $[1 1 1]$  ( $c^*$ ) direction as compared to the  $[\bar{1} 1 0]$  (or  $b$ ) direction.

Our results for the magnetization from NLCE are presented in Fig. 4, where  $M$  is defined as the total spin orientation along an external magnetic field  $M = \langle \vec{S} \rangle \cdot \vec{B} / B$ . To account for both of the previously described sources of anisotropy, we include a  $g$ -factor difference of  $g_{c^*} = 1.88$  versus  $g_b = 2.36$  [63] into 1, apart from the finite off-diagonal  $\Gamma$  interaction which we use for the parameters. The magnetization is calculated at a temperature of  $T \sim 30$  K. At this temperature and for  $B = 0$  the 10th and 11th order Euler sums are almost converged. Therefore, and since the out-of-plane magnetization remains featureless within the field range considered, we remain with NLCE at  $n_{max} = 10$ , while for the in-plane magnetization we display  $n_{max} = 11$  results. For comparison, we also show magnetization from ED, which we calculate on the 16 site cluster marked (d) in Fig. 3. In the out-of-plane case the agreement between NLCE and ED is excellent, whereas in the in-plane case, while still showing good agreement, the magnetization calculated by ED displays a slightly steeper slope for low magnetic field values. We mention, that increasing the magnetic field we find an improved convergence of the Euler resummation. This is due to the increasingly polarized state which can be captured on even smaller clusters.

Obviously the magnetization versus magnetic field which we find is highly anisotropic with the in-plane magnetization being around 7-10 times larger than the out-of-plane magnetization. As a consequence the susceptibility  $\partial M / \partial B$  is also anisotropic. Moreover, the in-plane magnetization starts to show saturation above approximately

15 T, while the out-of-plane magnetization remains linear up to 30 T. These results, i.e., strong anisotropy and different saturation behavior, agree very well with earlier studies using 24-site ED [63, 108] on microscopic models with additional interactions compared to the ones considered here, as well as experimental results [105].

#### D. Magnetostriction

Now that we have established that NLCE is capable of obtaining reliable results for basic thermodynamic properties of the  $J$ - $K$ - $\Gamma$  model, we turn to the magnetoelastic property of central interest to this work, namely the linear magnetostriction coefficient  $\lambda_{c^*}$ . This is defined by the relative change of length along the  $c^*$  direction due to the application of a magnetic field

$$\lambda_{c^*} = \frac{\partial \ln l_{c^*}}{\partial B}. \quad (8)$$

For the present model, magnetostriction stems from the fact that, to leading order, bond-stretching of the exchange paths leads to changes of the Hamiltonian which are proportional to spin-bilinears [109]. Therefore, reciprocally, manipulating the spin-correlations by application of an external magnetic field will induce changes of the bond lengths.

Thermodynamically, the differential of the Helmholtz free energy including anisotropic strain and stress reads

$$dF = -SdT + \int dr^3 \sigma_{ij} d\epsilon_{ij} - MdB \quad (9)$$

where  $S$  is the entropy,  $\sigma_{ij}$  and  $\epsilon_{ij}$  are the stress and strain tensors respectively. Assuming homogenous stress, the spatial integral yields the volume  $V$  of the crystal. Furthermore, discarding any trigonal distortion, model (1) displays  $C_3^*$  symmetry, comprising combined three-fold rotations in spin and real space. In turn, the stress and strain tensors are diagonal in a basis of principal axes containing  $c^*$ . In this basis we write

$$dF = -SdT + V\sigma_i d\epsilon_i - MdB \quad (10)$$

with diagonal elements  $\sigma_i \equiv \sigma_{ii}$ ,  $\epsilon_i \equiv \epsilon_{ii}$  for each principal axis ' $i$ '. The preceding assumption of  $C_3^*$  symmetry is merely used to simplify the elasticity analysis and is not meant to change the  $g$ -tensor anisotropy. In this work we consider uniaxial stress along  $i = c^*$ . Since  $d\epsilon_i = d \ln l_i$ , one obtains from Eq. (10) the Maxwell relation

$$\frac{\partial \ln l_{c^*}}{\partial B} = \frac{1}{V} \frac{\partial M}{\partial \sigma_{c^*}}. \quad (11)$$

Defining  $J_\alpha = \{J, K, \Gamma\}$  for  $\alpha=1,2,3$ , this can be expressed via the strain dependence of  $J_\alpha$ , i.e., exactly the magnetoelastic coupling, as

$$\lambda_{c^*} = \frac{1}{V} \sum_{\alpha} \frac{\partial M}{\partial J_\alpha} \frac{\partial J_\alpha}{\partial \sigma_{c^*}}, \quad (12)$$

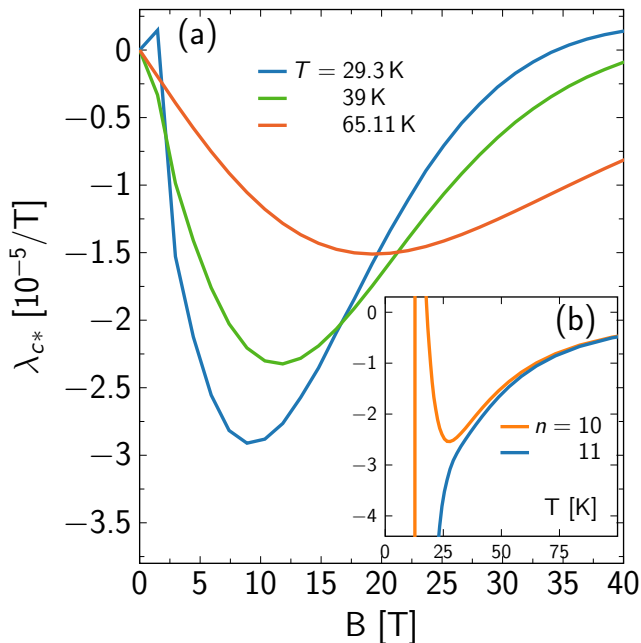


FIG. 5. (a) Linear magnetostriction coefficient  $\lambda_{c^*}$  of the  $J$ - $K$ - $\Gamma$  model from NLCE at 11th order versus in-plane magnetic field along the  $[\bar{1}10]$  direction for various temperatures. (b) Comparing NLCE for  $\lambda_{c^*}$  at 10th and 11th order (solid orange and blue) versus temperature at fixed  $B = 8.9$  T.

where  $\partial J_\alpha / \partial \sigma_{c^*}$  is of dimension  $[J]/\text{GPa}$  and to linear order is conventionally expressed using a parameter  $n_\alpha$  as  $n_\alpha J_\alpha$ , which leads to

$$\lambda_{c^*} = -\frac{1}{V} \sum_{\alpha} \left( \frac{\partial M}{\partial J_\alpha} n_\alpha J_\alpha \right). \quad (13)$$

For the values of  $n_\alpha$  in  $\alpha$ - $\text{RuCl}_3$  we rely on two inputs. I.e., we use results from *ab-initio* calculations under uniaxial pressure along  $c^*$  [63] which can be expressed as  $\{n_J, n_K, n_\Gamma\} = \{-0.283, -4.97, +1.0\} \times n_\Gamma \text{ GPa}^{-1}$  with  $n_\Gamma = 0.806$ . For  $n_\Gamma$ , however, and as suggested in [62], we use a slightly larger value of 0.9 instead, in order to improve the agreement with experimental values. Finally,  $V/N = 92.8 \text{ \AA}^3$ . Note that both, positive and negative values of  $n_\alpha$  occur.

We evaluate  $\lambda_{c^*}(B, T)$  by calculating the magnetization versus temperature, magnetic field, and  $J_\alpha$ , using NLCE and then approximating the derivative in Eq. (13) numerically

$$\frac{\partial M}{\partial J_\alpha} \approx \frac{M(J_\alpha + \Delta_\alpha) - M(J_\alpha)}{\Delta_\alpha}, \quad (14)$$

where we find a spacing of  $\Delta_\alpha = J_\alpha/100$  to be sufficiently small. Fig. 5(a) presents the resulting field dependence of  $\lambda_{c^*}$  at  $T = 29.3$  K, 39 K, and 65.11 K. Not to clutter the figure, the plots only show Euler transforms at the largest index we obtain, i.e.,  $n = 11$ . At this order NLCE is not fully converged for all temperatures and fields used

in 5(a). However, the margin of error is relatively small as can be read off from Fig. 5(b). This inset proves, that the uncertainty in  $\lambda_{c^*}(8.9 \text{ T})$  is at most  $O(10\%)$  at  $T \sim 29.3$  K and rapidly decreases with increasing temperature. Approaching full polarization also improves convergence of the expansion, which is relevant however only at magnetic field scales beyond 20 T in Fig. 5(a).

Most important, and as a main finding of this work, we observe a pronounced dip of  $\lambda_{c^*}$  versus magnetic field. As the temperature is lowered the dip sharpens up, deepens and its position moves to a field clearly similar to  $H_{c2}$ . Increasing the temperature the dip gets less pronounced and its location moves to higher fields. Qualitatively, these results regarding the field and temperature dependence of  $\lambda_{c^*}$  are in agreement with experiment [62, 64] and with earlier calculations using ED [63]. Also the magnitude of  $\lambda_{c^*}$  is within the experimentally observed range. We emphasize, however, that experiments have been performed for  $2.4 \text{ K} \leq T \leq 50 \text{ K}$ , while 11th-order NLCE's lowest reliable temperature is  $T \sim 24 \text{ K}$ , which is obvious from the inset Fig. 5(b). Substantially larger orders seem necessary to cover all of the experimental temperature range. *Cum grano salis* NLCE also agrees with conclusions from linear spin-wave calculations [62], which however, artificially, produces a divergent dip in  $\lambda_{c^*}(B, T)$  at  $H_{c2}$  for all temperatures.

## V. SUMMARY

We have shown the NLCE to be a promising tool to study thermodynamic properties of frustrated quantum magnets including magnetoelastic phenomena. For this purpose we have analyzed the  $J$ - $K$ - $\Gamma$  model of the Kitaev magnet  $\alpha$ - $\text{RuCl}_3$ , contrasting results from NLCE with ED where appropriate. We find the specific heat generated by NLCE to be in the thermodynamic limit over a wide range of temperatures on clusters which are much smaller than those for ED, which, in contrast, remain subject to finite size effects for all clusters we analyzed. The magnetization we obtained from NLCE displays a strong anisotropy with respect to the direction of the applied magnetic field, which is driven by the  $g$ -tensor anisotropy as well as the  $\Gamma$  interaction and is consistent with ED calculations and the experimental situation in  $\alpha$ - $\text{RuCl}_3$ .

Most important, we have used NLCE to investigate the linear magnetostriction coefficient along the  $c^*$ -axis and found a pronounced dip at a magnetic field which we associate with the field-driven transition out of the zigzag ordered phase at  $H_{c2}$  in  $\alpha$ - $\text{RuCl}_3$ . This, as well as the temperature dependence of the magnetostriction, is in good qualitative agreement with existing theoretical analysis as well as with experimental observations.

Finally, while our results are consistent with the location of the field-driven transition in  $\alpha$ - $\text{RuCl}_3$ , we cannot provide insight into the nature of the underlying phases. In particular regarding high fields beyond  $H_{c2}$  these re-

main under debate, despite extensive studies [22–26, 110]. Therefore, while it is well established that magnetic fields applied along the  $b$ -axis suppress the zigzag magnetic order, leading to a potentially spin-liquid-like state, the precise nature of this state and whether or not it is adiabatically connected to the high-field paramagnetic phases remain open issues.

## ACKNOWLEDGMENTS

Many stimulating discussions with Johannes Richter regarding the size-consistent cluster method for spin systems of Refs. [94–96] are gratefully acknowledged. This work has been supported in part by the DFG through Project A02 of SFB 1143 (Project-Id 247310070). Research of W.B. was supported in part by NSF grant PHY-2210452 to the Aspen Center for Physics (ACP). W.B. acknowledges kind hospitality of the PSM, Dresden.

- 
- [1] M. E. Lines, Elastic properties of magnetic materials, *Phys. Rep.* **55**, 133 (1979).
- [2] L. Zhu, M. Garst, A. Rosch, and Q. Si, Universally Diverging Grüneisen Parameter and the Magnetocaloric Effect Close to Quantum Critical Points, *Phys. Rev. Lett.* **91**, 066404 (2003).
- [3] M. C. Cross and D. S. Fisher, A new theory of the spin-Peierls transition with special relevance to the experiments on TTFCuBDT, *Phys. Rev. B* **19**, 402 (1979).
- [4] S. Zherlitsyn, S. Yasin, J. Wosnitzer, A. A. Zvyagin, A. V. Andreev, and V. Tsurkan, Spin-lattice effects in selected antiferromagnetic materials (Review Article), *Low Temp. Phys.* **40**, 123 (2014).
- [5] N. Tang, M. Gen, M. Rotter, H. Man, K. Matsuhira, A. Matsuo, K. Kindo, A. Ikeda, Y. H. Matsuda, P. Gegenwart, S. Nakatsuji, and Y. Kohama, Crystal field magnetostriction of spin ice under ultrahigh magnetic fields, *Phys. Rev. B* **110**, 214414 (2024).
- [6] T. Nomura, P. Corboz, A. Miyata, S. Zherlitsyn, Y. Ishii, Y. Kohama, Y. H. Matsuda, A. Ikeda, C. Zhong, H. Kageyama, and F. Mila, Unveiling new quantum phases in the Shastry-Sutherland compound  $\text{SrCu}_2(\text{BO}_3)_2$  up to the saturation magnetic field, *Nat. Commun.* **14**, 3769 (2023).
- [7] M. Gen, H. Ishikawa, A. Ikeda, A. Miyake, Z. Yang, Y. Okamoto, M. Mori, K. Takenaka, H. Sagayama, T. Kurumaji, Y. Tokunaga, T. Arima, M. Tokunaga, K. Kindo, Y. H. Matsuda, and Y. Kohama, Complex magnetic phase diagram with a small phase pocket in a three-dimensional frustrated magnet  $\text{CuInCr}_4\text{S}_8$ , *Phys. Rev. Research* **4**, 033148 (2022).
- [8] A. Miyata, T. Hikihara, S. Furukawa, R. K. Kremer, S. Zherlitsyn, and J. Wosnitzer, Magnetoelastic study on the frustrated quasi-one-dimensional spin- $\frac{1}{2}$  magnet  $\text{LiCuVO}_4$ , *Phys. Rev. B* **103**, 014411 (2021).
- [9] M. Doerr, T. Stöter, M. Rotter, and A. A. Zvyagin, Magnetostriction of the spin-ice system  $\text{Yb}_2\text{Ti}_2\text{O}_7$ , *J. Magn. Mater.* **449**, 378 (2018).
- [10] M. Jaime, R. Daou, S. A. Crooker, F. Weickert, A. Uchida, A. E. Feiguin, C. D. Batista, H. A. Dabkowska, and B. D. Gaulin, Magnetostriction and magnetic texture to 100.75 Tesla in frustrated  $\text{SrCu}_2(\text{BO}_3)_2$ , *Proc. Natl. Acad. Sci. U.S.A.* **109**, 12404 (2012).
- [11] J. Hemberger, H.-A. Krug von Nidda, V. Tsurkan, and A. Loidl, Large Magnetostriction and Negative Thermal Expansion in the Frustrated Antiferromagnet  $\text{ZnCr}_2\text{Se}_4$ , *Phys. Rev. Lett.* **98**, 147203 (2007).
- [12] A. Kitaev, Anyons in an exactly solved model and beyond, *Ann. Phys. (N. Y.)* **321**, 2 (2006).
- [13] H. Takagi, T. Takayama, G. Jackeli, G. Khaliullin, and S. E. Nagler, Concept and realization of Kitaev quantum spin liquids, *Nat. Rev. Phys.* **1**, 264 (2019).
- [14] Y. Motome and J. Nasu, Hunting Majorana Fermions in Kitaev Magnets, *J. Phys. Soc. Jpn.* **89**, 012002 (2020).
- [15] S. Trebst and C. Hickey, Kitaev materials, *Phys. Rep.* **950**, 1 (2022).
- [16] G. Baskaran, S. Mandal, and R. Shankar, Exact Results for Spin Dynamics and Fractionalization in the Kitaev Model, *Phys. Rev. Lett.* **98**, 247201 (2007).
- [17] G. Jackeli and G. Khaliullin, Mott Insulators in the Strong Spin-Orbit Coupling Limit: From Heisenberg to a Quantum Compass and Kitaev Models, *Phys. Rev. Lett.* **102**, 017205 (2009).
- [18] K. W. Plumb, J. P. Clancy, L. J. Sandilands, V. Vijay Shankar, Y. F. Hu, K. S. Burch, H.-Y. Kee, and Y.-J. Kim,  $\alpha\text{-RuCl}_3$ : A spin-orbit assisted Mott insulator on a honeycomb lattice, *Phys. Rev. B* **90**, 041112(R) (2014).
- [19] H. B. Cao, A. Banerjee, J.-Q. Yan, C. A. Bridges, M. D. Lumsden, D. G. Mandrus, D. A. Tennant, B. C. Chakoumakos, and S. E. Nagler, Low-temperature crystal and magnetic structure of  $\alpha\text{-RuCl}_3$ , *Phys. Rev. B* **93**, 134423 (2016).
- [20] J. A. Sears, Y. Zhao, Z. Xu, J. W. Lynn, and Y.-J. Kim, Phase diagram of  $\alpha\text{-RuCl}_3$  in an in-plane magnetic field, *Phys. Rev. B* **95**, 180411(R) (2017).
- [21] A. U. B. Wolter, L. T. Corredor, L. Janssen, K. Nenkov, S. Schönecker, S.-H. Do, K.-Y. Choi, R. Albrecht, J. Hunger, T. Doert, M. Vojta, and B. Büchner, Field-induced quantum criticality in the Kitaev system  $\alpha\text{-RuCl}_3$ , *Phys. Rev. B* **96**, 041405(R) (2017).
- [22] S.-H. Baek, S.-H. Do, K.-Y. Choi, Y. S. Kwon, A. U. B. Wolter, S. Nishimoto, J. van den Brink, and B. Büchner, Evidence for a Field-Induced Quantum Spin Liquid in  $\alpha\text{-RuCl}_3$ , *Phys. Rev. Lett.* **119**, 037201 (2017).
- [23] R. Hentrich, A. U. B. Wolter, X. Zotos, W. Brenig, D.

- Nowak, A. Isaeva, T. Doert, A. Banerjee, P. Lampen-Kelley, D. G. Mandrus, S. E. Nagler, J. Sears, Y.-J. Kim, B. Büchner, and C. Hess, Unusual Phonon Heat Transport in  $\alpha$ -RuCl<sub>3</sub>: Strong Spin-Phonon Scattering and Field-Induced Spin Gap, *Phys. Rev. Lett.* **120**, 117204 (2018).
- [24] C. Balz, P. Lampen-Kelley, A. Banerjee, J. Yan, Z. Lu, X. Hu, S. M. Yadav, Y. Takano, Y. Liu, D. A. Tennant, M. D. Lumsden, D. Mandrus, and S. E. Nagler, Finite field regime for a quantum spin liquid in  $\alpha$ -RuCl<sub>3</sub>, *Phys. Rev. B* **100**, 060405(R) (2019).
- [25] R. Schönemann, S. Imajo, F. Weickert, J. Yan, D. G. Mandrus, Y. Takano, E. L. Brosha, P. F. S. Rosa, S. E. Nagler, K. Kindo, and M. Jaime, Thermal and magnetoelastic properties of  $\alpha$ -RuCl<sub>3</sub> in the field-induced low-temperature states, *Phys. Rev. B* **102**, 214432 (2020).
- [26] C. Balz, L. Janssen, P. Lampen-Kelley, A. Banerjee, Y. H. Liu, J.-Q. Yan, D. G. Mandrus, M. Vojta, and S. E. Nagler, Field-induced intermediate ordered phase and anisotropic interlayer interactions in  $\alpha$ -RuCl<sub>3</sub>, *Phys. Rev. B* **103**, 174417 (2021).
- [27] L. J. Sandilands, Y. Tian, K. W. Plumb, Y.-J. Kim, and K. S. Burch, Scattering Continuum and Possible Fractionalized Excitations in  $\alpha$ -RuCl<sub>3</sub>, *Phys. Rev. Lett.* **114**, 147201 (2015).
- [28] J. Nasu, J. Knolle, D. L. Kovrizhin, Y. Motome, and R. Moessner, Fermionic response from fractionalization in an insulating two-dimensional magnet, *Nat. Phys.* **12**, 912 (2016).
- [29] D. Wulferding, Y. Choi, S.-H. Do, C. H. Lee, P. Lemmens, C. Faugeras, Y. Gallais, and K.-Y. Choi, Magnon bound states versus anyonic Majorana excitations in the Kitaev honeycomb magnet  $\alpha$ -RuCl<sub>3</sub>, *Nat. Commun.* **11**, 1 (2020).
- [30] J. Knolle, D. L. Kovrizhin, J. T. Chalker, and R. Moessner, Dynamics of a Two-Dimensional Quantum Spin Liquid: Signatures of Emergent Majorana Fermions and Fluxes, *Phys. Rev. Lett.* **112**, 207203 (2014).
- [31] A. Banerjee, C. A. Bridges, J.-Q. Yan, A. A. Aczel, L. Li, M. B. Stone, G. E. Granroth, M. D. Lumsden, Y. Yiu, J. Knolle, S. Bhattacharjee, D. L. Kovrizhin, R. Moessner, D. A. Tennant, D. G. Mandrus, and S. E. Nagler, Proximate Kitaev quantum spin liquid behaviour in a honeycomb magnet, *Nat. Mater.* **15**, 733 (2016).
- [32] A. Banerjee, J. Yan, J. Knolle, C. A. Bridges, M. B. Stone, M. D. Lumsden, D. G. Mandrus, D. A. Tennant, R. Moessner, and S. E. Nagler, Neutron scattering in the proximate quantum spin liquid  $\alpha$ -RuCl<sub>3</sub>, *Science* **356**, 1055 (2017).
- [33] S.-H. Do, S.-Y. Park, J. Yoshitake, J. Nasu, Y. Motome, Y. S. Kwon, D. T. Adroja, D. J. Voneshen, K. Kim, T.-H. Jang, J.-H. Park, K.-Y. Choi, and S. Ji, Majorana fermions in the Kitaev quantum spin system  $\alpha$ -RuCl<sub>3</sub>, *Nat. Phys.* **13**, 1079 (2017).
- [34] G. B. Halász, N. B. Perkins, and J. van den Brink, Resonant Inelastic X-Ray Scattering Response of the Kitaev Honeycomb Model, *Phys. Rev. Lett.* **117**, 127203 (2016).
- [35] A. Metavitsiadis and W. Brenig, Phonon renormalization in the Kitaev quantum spin liquid, *Phys. Rev. B* **101**, 035103 (2020).
- [36] M. Ye, R. M. Fernandes, and N. B. Perkins, Phonon dynamics in the Kitaev spin liquid, *Phys. Rev. Research* **2**, 033180 (2020).
- [37] K. Feng, M. Ye, and N. B. Perkins, Temperature evolution of the phonon dynamics in the Kitaev spin liquid, *Phys. Rev. B* **103**, 214416 (2021).
- [38] H. Li, T. T. Zhang, A. Said, G. Fabbris, D. G. Mazzone, J. Q. Yan, D. Mandrus, G. B. Halász, S. Okamoto, S. Murakami, M. P. M. Dean, H. N. Lee, and H. Miao, Giant phonon anomalies in the proximate Kitaev quantum spin liquid  $\alpha$ -RuCl<sub>3</sub>, *Nat. Commun.* **12**, 3513 (2021).
- [39] K. Feng, S. Swarup, and N. B. Perkins, Footprints of Kitaev spin liquid in the Fano lineshape of Raman-active optical phonons, *Phys. Rev. B* **105**, L121108 (2022).
- [40] A. Metavitsiadis, W. Natori, J. Knolle, and W. Brenig, Optical phonons coupled to a Kitaev spin liquid, *Phys. Rev. B* **105**, 165151 (2022).
- [41] S. Singh, P. P. Stavropoulos, and N. B. Perkins, Phonon dynamics in the generalized Kitaev spin liquid, *Phys. Rev. B* **107**, 214428 (2023).
- [42] A. Hauspurg, S. Zherlitsyn, T. Helm, V. Felea, J. Wosnitza, V. Tsurkan, K.-Y. Choi, S.-H. Do, M. Ye, W. Brenig, and N. B. Perkins, Fractionalized excitations probed by ultrasound, *Phys. Rev. B* **109**, 144415 (2024).
- [43] A. Hauspurg, S. Singh, T. Yanagisawa, V. Tsurkan, J. Wosnitza, W. Brenig, N. B. Perkins, and S. Zherlitsyn, Spin-strain interactions under hydrostatic pressure in  $\alpha$ -RuCl<sub>3</sub>, arXiv:2503.04656.
- [44] H.-S. Kim, V. Vijay Shankar, A. Catuneanu, and H.-Y. Kee, Kitaev magnetism in honeycomb RuCl<sub>3</sub> with intermediate spin-orbit coupling, *Phys. Rev. B* **91**, 241110(R) (2015).
- [45] H.-S. Kim and H.-Y. Kee, Crystal structure and magnetism in  $\alpha$ -RuCl<sub>3</sub> : An *ab initio* study, *Phys. Rev. B* **93**, 155143 (2016).
- [46] S. M. Winter, Y. Li, H. O. Jeschke, and R. Valentí, Challenges in design of Kitaev materials: Magnetic interactions from competing energy scales, *Phys. Rev. B* **93**, 214431 (2016).
- [47] S. M. Winter, K. Riedl, P. A. Maksimov, A. L. Chernyshev, A. Honecker, and R. Valentí, Breakdown of magnons in a strongly spin-orbital coupled magnet, *Nat. Commun.* **8**, 1152 (2017).
- [48] K. Ran, J. Wang, W. Wang, Z.-Y. Dong, X. Ren, S. Bao, S. Li, Z. Ma, Y. Gan, Y. Zhang, J. T. Park, G. Deng, S. Danilkin, S.-L. Yu, J.-X. Li, and J. Wen, Spin-Wave Excitations Evidencing the Kitaev Interaction in Single Crystalline  $\alpha$ -RuCl<sub>3</sub>, *Phys. Rev. Lett.* **118**, 107203 (2017).
- [49] L. Janssen, E. C. Andrade, and M. Vojta, Magnetization processes of zigzag states on the honeycomb lattice: Identifying spin models for  $\alpha$ -RuCl<sub>3</sub> and Na<sub>2</sub>IrO<sub>3</sub>, *Phys. Rev. B* **96**, 064430 (2017).
- [50] W. Wang, Z.-Y. Dong, S.-L. Yu, and J.-X. Li, Theoretical investigation of magnetic dynamics in  $\alpha$ -RuCl<sub>3</sub>, *Phys. Rev. B* **96**, 115103 (2017).
- [51] T. Cookmeyer and J. E. Moore, Spin-wave analysis of the low-temperature thermal Hall effect in the candidate Kitaev spin liquid  $\alpha$ -RuCl<sub>3</sub>, *Phys. Rev. B* **98**, 060412(R) (2018).
- [52] L. Wu, A. Little, E. E. Aldape, D. Rees, E. Thewalt, P. Lampen-Kelley, A. Banerjee, C. A. Bridges, J.-Q. Yan, D. Boone, S. Patankar, D. Goldhaber-Gordon, D. Mandrus, S. E. Nagler, E. Altman, and J. Orenstein, Field evolution of magnons in  $\alpha$ -RuCl<sub>3</sub> by high-resolution polarized terahertz spectroscopy, *Phys. Rev. B* **98**, 094425 (2018).



- [53] I. O. Ozel, C. A. Belvin, E. Baldini, I. Kimchi, S.-H. Do, K.-Y. Choi, and N. Gedik, Magnetic field-dependent low-energy magnon dynamics in  $\alpha$ -RuCl<sub>3</sub>, *Phys. Rev. B* **100**, 085108 (2019).
- [54] L. Janssen and M. Vojta, Heisenberg-Kitaev physics in magnetic fields, *J. Phys.: Condens. Matter* **31**, 423002 (2019).
- [55] E. C. Andrade, L. Janssen, and M. Vojta, Susceptibility anisotropy and its disorder evolution in models for Kitaev materials, *Phys. Rev. B* **102**, 115160 (2020).
- [56] C. Kim, H.-S. Kim, and J.-G. Park, Spin-orbital entangled state and realization of Kitaev physics in 3d cobalt compounds: a progress report, *J. Phys.: Condens. Matter* **34**, 023001 (2022).
- [57] I. Rousochatzakis, N. B. Perkins, Q. Luo, and H.-Y. Kee, Beyond Kitaev physics in strong spin-orbit coupled magnets, *Rep. Prog. Phys.* **87**, 026502 (2024).
- [58] M. Möller, P. A. Maksimov, S. Jiang, S. R. White, R. Valentí, and A. L. Chernyshev, Rethinking  $\alpha$ -RuCl<sub>3</sub>: Parameters, models, and phase diagram, *Phys. Rev. B* **112**, 104403 (2025).
- [59] R. Hentrich, M. Roslova, A. Isaeva, T. Doert, W. Brenig, B. Büchner, and C. Hess, Large thermal Hall effect in  $\alpha$ -RuCl<sub>3</sub>: Evidence for heat transport by Kitaev-Heisenberg paramagnons, *Phys. Rev. B* **99**, 085136 (2019).
- [60] Y. Vinkler-Aviv and A. Rosch, Approximately Quantized Thermal Hall Effect of Chiral Liquids Coupled to Phonons, *Phys. Rev. X* **8**, 031032 (2018).
- [61] M. Ye, G. B. Halász, L. Savary, and L. Balents, Quantization of the Thermal Hall Conductivity at Small Hall Angles, *Phys. Rev. Lett.* **121**, 147201 (2018).
- [62] S. Gass, P. M. Cönsoli, V. Kocsis, L. T. Corredor, P. Lampen-Kelley, D. G. Mandrus, S. E. Nagler, L. Janssen, M. Vojta, B. Büchner, and A. U. B. Wolter, Field-induced transitions in the Kitaev material  $\alpha$ -RuCl<sub>3</sub> probed by thermal expansion and magnetostriction, *Phys. Rev. B* **101**, 245158 (2020).
- [63] D. A. S. Kaib, S. Biswas, K. Riedl, S. M. Winter, and R. Valentí, Magnetoelastic coupling and effects of uniaxial strain in  $\alpha$ -RuCl<sub>3</sub> from first principles, *Phys. Rev. B* **103**, L140402 (2021).
- [64] V. Kocsis, D. A. S. Kaib, K. Riedl, S. Gass, P. Lampen-Kelley, D. G. Mandrus, S. E. Nagler, N. Pérez, K. Nielsch, B. Büchner, A. U. B. Wolter, and R. Valentí, Magnetoelastic coupling anisotropy in the Kitaev material  $\alpha$ -RuCl<sub>3</sub>, *Phys. Rev. B* **105**, 094410 (2022).
- [65] M. Rigol, T. Bryant, and R. R. P. Singh, Numerical Linked-Cluster Approach to Quantum Lattice Models, *Phys. Rev. Lett.* **97**, 187202 (2006).
- [66] M. Rigol, T. Bryant, and R. R. P. Singh, Numerical linked-cluster algorithms. I. Spin systems on square, triangular, and kagomé lattices, *Phys. Rev. E* **75**, 061118 (2007).
- [67] J. Oitmaa, C. Hamer, and W. Zheng, *Series Expansion Methods for Strongly Interacting Lattice Models* (Cambridge University Press, 2006).
- [68] M. F. Sykes, J. W. Essam, B. R. Heap, and B. J. Hiley, Lattice Constant Systems and Graph Theory, *J. Math. Phys.* **7**, 1557 (1966).
- [69] R. R. P. Singh and J. Oitmaa, Corrections to Pauling residual entropy and single tetrahedron based approximations for the pyrochlore lattice Ising antiferromagnet, *Phys. Rev. B* **85**, 144414 (2012).
- [70] D. Ixert and K. P. Schmidt, Nonperturbative linked-cluster expansions in long-range ordered quantum systems, *Phys. Rev. B* **94**, 195133 (2016).
- [71] E. Khatami and M. Rigol, Thermodynamics of the antiferromagnetic Heisenberg model on the checkerboard lattice, *Phys. Rev. B* **83**, 134431 (2011).
- [72] E. Khatami, R. R. P. Singh, and M. Rigol, Thermodynamics and phase transitions for the Heisenberg model on the pinwheel distorted kagome lattice, *Phys. Rev. B* **84**, 224411 (2011).
- [73] E. Khatami, J. S. Helton, and M. Rigol, Numerical study of the thermodynamics of clinoptacumite, *Phys. Rev. B* **85**, 064401 (2012).
- [74] N. R. Hayre, K. A. Ross, R. Applegate, T. Lin, R. R. P. Singh, B. D. Gaulin, and M. J. P. Gingras, Thermodynamic properties of Yb<sub>2</sub>Ti<sub>2</sub>O<sub>7</sub> pyrochlore as a function of temperature and magnetic field: Validation of a quantum spin ice exchange Hamiltonian, *Phys. Rev. B* **87**, 184423 (2013).
- [75] R. Schäfer, I. Hagymási, R. Moessner, and D. J. Luitz, Pyrochlore  $S=1/12$  Heisenberg antiferromagnet at finite temperature, *Phys. Rev. B* **102**, 054408 (2020).
- [76] K. Mallayya and M. Rigol, Numerical linked cluster expansions for quantum quenches in one-dimensional lattices, *Phys. Rev. E* **95**, 033302 (2017).
- [77] J. Richter, T. Heitmann, and R. Steinigeweg, Quantum quench dynamics in the transverse-field Ising model: A numerical expansion in linked rectangular clusters, *SciPost Phys.* **9**, 031 (2020).
- [78] A. B. Kallin, K. Hyatt, R. R. P. Singh, and R. G. Melko, Entanglement at a Two-Dimensional Quantum Critical Point: A Numerical Linked-Cluster Expansion Study, *Phys. Rev. Lett.* **110**, 135702 (2013).
- [79] A. B. Kallin, E. M. Stoudenmire, P. Fendley, R. R. P. Singh, and R. G. Melko, Corner contribution to the entanglement entropy of an  $O(3)$  quantum critical point in  $2 + 1$  dimensions, *J. Stat. Mech.* **2014**, P06009 (2014).
- [80] R. Applegate, N. R. Hayre, R. R. P. Singh, T. Lin, A. G. R. Day, and M. J. P. Gingras, Vindication of Yb<sub>2</sub>Ti<sub>2</sub>O<sub>7</sub> as a Model Exchange Quantum Spin Ice, *Phys. Rev. Lett.* **09**, 097205 (2012).
- [81] L. D. C. Jaubert, O. Benton, J. G. Rau, J. Oitmaa, R. R. P. Singh, N. Shannon, and M. J. P. Gingras, Are Multiphase Competition and Order by Disorder the Keys to Understanding Yb<sub>2</sub>Ti<sub>2</sub>O<sub>7</sub>?, *Phys. Rev. Lett.* **115**, 267208 (2015).
- [82] O. Benton, L. D. C. Jaubert, R. R. P. Singh, J. Oitmaa, and N. Shannon, Quantum Spin Ice with Frustrated Transverse Exchange: From a  $\pi$ -Flux Phase to a Nematic Quantum Spin Liquid, *Phys. Rev. Lett.* **121**, 067201 (2018).
- [83] T. Pardini, A. Menon, S. P. Hau-Riege, and R. R. P. Singh, Local entanglement and confinement transitions in the random transverse-field Ising model on the pyrochlore lattice, *Phys. Rev. B* **100**, 144437 (2019).
- [84] E. Khatami and M. Rigol, Thermodynamics of strongly interacting fermions in two-dimensional optical lattices, *Phys. Rev. A* **84**, 053611 (2011).
- [85] E. Khatami and M. Rigol, Effect of particle statistics in strongly correlated two-dimensional Hubbard models, *Phys. Rev. A* **86**, 023633 (2012).
- [86] E. Khatami and M. Rigol, Accessing the Mott Regime in 2D Optical Lattices with Strongly Interacting Fermions, *J. Supercond. Nov. Magn.* **25**, 2145 (2012).

- [87] R. A. Hart, P. M. Duarte, T.-L. Yang, X. Liu, T. Paiva, E. Khatami, R. T. Scalettar, N. Trivedi, D. A. Huse, and R. G. Hulet, Observation of antiferromagnetic correlations in the Hubbard model with ultracold atoms, *Nature* **519**, 211 (2015).
- [88] J. Gan and K. R. A. Hazzard, Numerical linked cluster expansions for inhomogeneous systems, *Phys. Rev. A* **102**, 013318 (2020).
- [89] M. Abdelshafy and M. Rigol, Numerical linked-cluster expansions for two-dimensional spin models with continuous disorder distributions, *Phys. Rev. E* **109**, 054127 (2024).
- [90] H. Y. Yang and K. P. Schmidt, Effective models for gapped phases of strongly correlated quantum lattice models, *EPL* **94**, 17004 (2011).
- [91] B. Tang, E. Khatami, and M. Rigol, A short introduction to numerical linked-cluster expansions, *Comput. Phys. Commun.* **184**, 557 (2013).
- [92] O. Benton, Instabilities of a U(1) Quantum Spin Liquid in Disordered Non-Kramers Pyrochlores, *Phys. Rev. Lett.* **121**, 037203 (2018).
- [93] Sumeet, M. Hörmann, and K. P. Schmidt, Hybrid quantum-classical algorithm for the transverse-field Ising model in the thermodynamic limit, *Phys. Rev. B* **110**, 155128 (2024).
- [94] R. F. Bishop, D. J. J. Farnell, S. E. Krüger, J. B. Parkinson, J. Richter, and C. Zeng, High-order coupled cluster method calculations for the ground- and excited-state properties of the spin-half XXZ model, *J. Phys.: Condens. Matter* **12**, 6887 (2000).
- [95] D. J. J. Farnell, R. Zinke, J. Schulenburg, and J. Richter, High-order coupled cluster method study of frustrated and unfrustrated quantum magnets in external magnetic fields, *J. Phys.: Condens. Matter* **21**, 406002 (2009).
- [96] J. Reuther, P. Wölfle, R. Darradi, W. Brenig, M. Arlego, and J. Richter, Quantum phases of the planar antiferromagnetic  $J_1$ - $J_2$ - $J_3$  Heisenberg model, *Phys. Rev. B* **83**, 064416 (2011).
- [97] J. G. Rau, E. K.-H. Lee, and H.-Y. Kee, Generic Spin Model for the Honeycomb Iridates beyond the Kitaev Limit, *Phys. Rev. Lett.* **112**, 077204 (2014).
- [98] B. D. McKay and A. Piperno, Practical graph isomorphism, II, *J. Symb. Comput.* **60**, 94 (2014).
- [99] E. J. Weniger, Nonlinear sequence transformations for the acceleration of convergence and the summation of divergent series, *Comput. Phys. Rep.* **10**, 189 (1989).
- [100] Y. Yamaji, T. Suzuki, T. Yamada, S. Suga, N. Kawashima, and M. Imada, Clues and criteria for designing a Kitaev spin liquid revealed by thermal and spin excitations of the honeycomb iridate  $\text{Na}_2\text{IrO}_3$ , *Phys. Rev. B* **93**, 174425 (2016).
- [101] J. Nasu, M. Udagawa, and Y. Motome, Vaporization of Kitaev Spin Liquids, *Phys. Rev. Lett.* **113**, 197205 (2014).
- [102] A. Pidatella, A. Metavitsiadis, and W. Brenig, Heat transport in the anisotropic Kitaev spin liquid, *Phys. Rev. B* **99**, 075141 (2019).
- [103] A. M. Samarakoon, G. Wachtel, Y. Yamaji, D. A. Tennant, C. D. Batista, and Y. B. Kim, Classical and quantum spin dynamics of the honeycomb  $\Gamma$  model, *Phys. Rev. B* **98**, 045121 (2018).
- [104] A. Catuneanu, Y. Yamaji, G. Wachtel, Y. B. Kim, and H.-Y. Kee, Path to stable quantum spin liquids in spin-orbit coupled correlated materials, *npj Quantum Mater.* **3**, 23 (2018).
- [105] R. D. Johnson, S. C. Williams, A. A. Haghighirad, J. Singleton, V. Zapf, P. Manuel, I. I. Mazin, Y. Li, H. O. Jeschke, R. Valentí, and R. Coldea, Monoclinic crystal structure of  $\alpha$ - $\text{RuCl}_3$  and the zigzag antiferromagnetic ground state, *Phys. Rev. B* **92**, 235119 (2015).
- [106] P. Lampen-Kelley, S. Rachel, J. Reuther, J.-Q. Yan, A. Banerjee, C. A. Bridges, H. B. Cao, S. E. Nagler, and D. Mandrus, Anisotropic susceptibilities in the honeycomb Kitaev system  $\alpha$ - $\text{RuCl}_3$ , *Phys. Rev. B* **98**, 100403 (2018).
- [107] Y. Kubota, H. Tanaka, T. Ono, Y. Narumi, and K. Kindo, Successive magnetic phase transitions in  $\alpha$ - $\text{RuCl}_3$ : XY-like frustrated magnet on the honeycomb lattice, *Phys. Rev. B* **91**, 094422 (2015).
- [108] S. M. Winter, K. Riedl, D. Kaib, R. Coldea, and R. Valentí, Probing  $\alpha$ - $\text{RuCl}_3$  Beyond Magnetic Order: Effects of Temperature and Magnetic Field, *Phys. Rev. Lett.* **120**, 077203 (2018).
- [109] V. S. Zapf, V. F. Correa, P. Sengupta, C. D. Batista, M. Tsukamoto, N. Kawashima, P. Egan, C. Pantea, A. Migliori, J. B. Betts, M. Jaime, and A. Paduan-Filho, Direct measurement of spin correlations using magnetostriiction, *Phys. Rev. B* **77**, 020404 (2008).
- [110] C. Hickey and S. Trebst, Emergence of a field-driven U(1) spin liquid in the Kitaev honeycomb model, *Nat. Commun.* **10**, 1 (2019).